Environmental Science & Technology

pubs.acs.org/est

Article

Temperature-Dependent Evaporative Anthropogenic VOC Emissions Significantly Exacerbate Regional Ozone Pollution

Wenlu Wu, Tzung-May Fu,* Steve R. Arnold,* Dominick V. Spracklen, Aoxing Zhang, Wei Tao, Xiaolin Wang, Yue Hou, Jiajia Mo, Jiongkai Chen, Yumin Li, Xu Feng, Haipeng Lin, Zhijiong Huang, Junyu Zheng, Huizhong Shen, Lei Zhu, Chen Wang, Jianhuai Ye, and Xin Yang

Cite This: *Environ. Sci. Technol.* 2024, 58, 5430−5441

Read Online

ACCESS | Metrics & More | Article Recommendations | Supporting Information

ABSTRACT: The evaporative emissions of anthropogenic volatile organic compounds (AVOCs) are sensitive to ambient temperature. This sensitivity forms an air pollution-meteorology connection that has not been assessed on a regional scale. We parametrized the temperature dependence of evaporative AVOC fluxes in a regional air quality model and evaluated the impacts on surface ozone in the Beijing−Tianjin−Hebei (BTH) area of China during the summer of 2017. The temperature dependency of AVOC emissions drove an enhanced simulated ozone-temperature sensitivity of 1.0 to 1.8 $\mu g\ m^{-3}\ K^{-1}$, comparable to the simulated ozone-temperature sensitivity driven by the temperature dependency of biogenic VOC emissions (1.7 to 2.4 $\mu g\ m^{-3}\ K^{-1}$). Ozone enhancements driven by temperature-induced AVOC increases were localized to their point of emission and were relatively more important in urban areas than in rural regions. The inclusion of the temperature-dependent AVOC emissions in our model improved the simulated ozone-temperature sensitivities on days of ozone exceedance. Our results demonstrated the importance of temperature-dependent AVOC emissions on surface ozone pollution and its heretofore unrepresented role in air pollution−meteorology interactions.

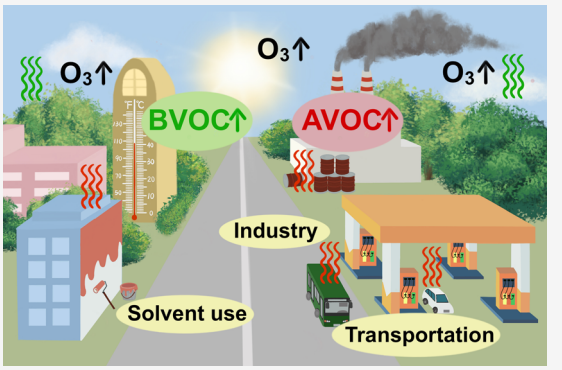

KEYWORDS: *anthropogenic emissions, volatile organic compounds, surface ozone, air quality, WRF-GC*

1. INTRODUCTION

Surface ozone, produced by the photochemical oxidation of volatile organic compounds (VOCs) in the presence of nitrogen oxides (NO_x = NO + NO_2), is a growing concern in China during the warm season. For example, in the Beijing−Tianjin−Hebei (BTH) area of China, the maximum daily 8 h average (MDA8) surface ozone concentrations exceeded the national standard of 160 $\mu g\ m^{-3}$ on 10 days in 2013,[1,2] but the number of exceedance days increased to 83 days in 2019.[3,4] It is thus imperative to better understand the mechanisms by which surface ozone pollution occurs in Chinese cities in order to develop more effective control strategies. VOCs that contribute to surface ozone pollution originate from a variety of anthropogenic, biogenic, and biomass-burning sources.[5] Among these sources, the emissions of biogenic VOCs (BVOCs), including, most importantly, isoprene, exacerbate ozone pollution events. This is because the warm and sunny conditions that facilitate ozone photochemical production also enhance BVOC emissions.[6] This meteorology-chemistry connection is well understood and is accounted for in most air quality models.[7]

In contrast, the emissions of anthropogenic VOCs (AVOCs) are also sensitive to ambient temperature; however, the potential impacts of this sensitivity on regional surface ozone have not been fully explored. Temperature variations affect both the intensities of anthropogenic activities and the emission factors of AVOCs from those activities. For instance, power generation increases at both high and low ambient temperatures due to power demands for cooling and heating. This weather-driven variation of anthropogenic activities has been accounted for in emission inventories on monthly to seasonal scales. Much less is known about the temperature dependence of AVOC emission factors, particularly the enhanced evaporation of AVOCs in warm weather. Many studies have shown that high ambient temperatures substantially increased the fugitive evaporative emissions of AVOCs from petrochemical processing, vehicles, as well as the use of solvents (e.g., painting/coating, dry cleaning, and print-

Received: November 2, 2023
Revised: January 27, 2024
Accepted: February 23, 2024
Published: March 12, 2024

ing[8−13]). Niu et al.[10] observed that in summer, the ambient levels of VOCs and oxygenated VOCs (OVOCs) associated with printing and dry cleaning were 20−40 times higher than their respective winter levels in a central Chinese city. Since the volatility of AVOC species varies, the temperature dependency of evaporative AVOC emissions also affects the composition and reactivity of AVOCs in the ambient air.[14] Na et al.[15] observed that warm weather enhanced the evaporative emissions of aromatics from vehicles in Seoul, Korea, and that the ozone formation potential (OFP) of VOCs from vehicular evaporative emissions was 40% higher than that from vehicular exhaust gases in summer. Gu et al.[16] incorporated into a box model a 1% increase of AVOC emissions per 3 °C rise in ambient temperature and found that this temperature dependence of AVOCs increased the simulated surface ozone concentrations by 2 ppb in urban Shanghai when the daily maximum temperature was 41 °C.

To the best of our knowledge, the impacts of temperature-dependent evaporative AVOC emissions on surface ozone have not been quantified on a regional scale. The main challenge was that the temperature dependency of AVOCs emitted from different sources has not been formulated and represented in regional models. In this study, we developed parametrizations for the temperature dependencies of evaporative AVOC emissions from transportation, solvent use, and other nonsolvent-use industrial activities (hereafter referred to as "NSI activities"). We tested these parametrizations to a regional air quality model to evaluate the responses of summertime surface ozone to temperature-dependent AVOC emissions in the BTH area of China. Finally, we compared the simulated ozone-temperature sensitivities driven by evaporative AVOC emissions and BVOC emissions, respectively, to better understand the role of temperature-dependent emissions in regional air quality−meteorology interactions.

2. METHODOLOGY

2.1. Simulations of Surface Ozone in the BTH Area Using the WRF-GC Model. We used the WRF-GC regional air quality model (v2.0)[17,18] to simulate surface ozone concentrations over China. WRF-GC is an online coupling of the Weather Research and Forecasting (WRF v3.9.1.1, https://www.mmm.ucar.edu/models/wrf)[19] meteorological model and the GEOS-Chem atmospheric chemistry model (v12.8.1, http://www.geos-chem.org/).[20] Our simulations were between May 28 and July 5, 2017, with the first 4 days of the simulation considered as model spin-up and discounted from analyses. We chose to simulate this period because June and July are the months with the most frequent ozone exceedances over the BTH area, although evaporative AVOC emissions are sensitive to temperature in all seasons. Also, the constraint for temperature dependency of NSI emissions was based on a most recent published observation in 2017.[14] We simulated a single domain of 27 km horizontal resolution and 50 vertical layers (Figure S1). WRF-GC used the O_3−VOC−NO_x−aerosol−halogen chemical mechanism from GEOS-Chem v12.8.1, which we supplemented with the photochemical mechanism of aromatics from GEOS-Chem v13.0.0.[5,21] Meteorological initial and boundary conditions were from the National Center for Environmental Prediction Final Operational Global Analysis (NCEP FNL, 1° resolution).[22] The simulated winds, temperature, and water vapor mixing ratios above the planetary boundary layer were nudged with the NCEP FNL data every 6 h. Aerosol feedback to meteorology was disabled to further ensure that the meteorological conditions in all simulations were identical. Chemical boundary conditions were from a standard full-chemistry simulation using GEOS-Chem v12.8.1.[20] Table S1 summarizes the physical configurations used in our simulations.

Monthly mean anthropogenic pollutant emissions within Mainland China were from the Multi-resolutionEmission Inventory for China (MEIC, http://www.meicmodel.org) for the year 2017, which included emissions from power generation, industries (distinguishing the solvent-use and nonsolvent-use subsectors), transportation (including on-road and off-road), and residential activities at 0.25° resolution.[23,24] Anthropogenic emissions for the rest of the simulated domain were from a mosaic Asian anthropogenic emission inventory for the year 2010.[25] Biomass-burning emissions were from the Global Fire Emissions Database version 4.1 with small fires (GFED4s).[26] Meteorology-dependent BVOC emissions (MEGAN v2.1)[6] and soil- and lightning-NO_x emissions[27,28] were calculated online in WRF-GC. Figure S2 shows the monthly mean VOC emissions over the BTH area during the simulation period. AVOC emissions from transportation, solvent use, and NSI activities generally overlapped in space, reflecting the collocation of the population, vehicles, and industrial activities over this area. The BVOC emissions were highest over Beijing, Tianjin, and the northeastern parts of Hebei, reflecting the denser vegetation in these areas relative to other parts of the BTH.

We conducted three sensitivity simulations to elucidate the impacts of temperature-dependent VOC emissions on surface ozone (Table S2). The BASE simulation was driven by meteorology-dependent BVOC emissions as well as temperature-independent AVOC emissions with prescribed weekday/weekend and diurnal temporal patterns to represent the anthropogenic activity variations independent of daily meteorological variations. The AVOC(T) simulation was identical to the BASE simulation, except that the hourly AVOC emissions were further dependent on hourly ambient temperature, as described in Section 2.2. We also conducted a BVOC(NT) simulation, which was identical to the BASE simulation, except the dependence of BVOC emissions on daily temperature variations was disabled. Instead, BVOC emissions were driven by the monthly mean temperature for each model grid. The simulated ozone differences between the AVOC(T) and the BASE experiments represented the impacts of temperature-dependent evaporative AVOC emissions, while the simulated ozone differences between the BASE and BVOC(NT) experiments represented the impacts of temperature-dependent BVOC emissions.

2.2. Parametrizations for the Temperature Dependency of Evaporative AVOC Emissions for Use in a Regional Air Quality Model. Several studies have derived the theoretical or empirical temperature dependence of evaporative VOC emissions from different anthropogenic sources.[29,30] Evaporative AVOC emissions from transportation mostly involved the vapor losses from bulk storage devices[31]; these evaporative fluxes took the form of eq 1,[29,30,32−35] analogous to the Clausius−Clapeyron equation:

$$E_1 = \frac{A_1}{T}\exp\left(\frac{-B_1}{T}\right) \quad (1)$$

where E_1 is the evaporative VOC emission flux from transportation (unit: kg m^{-2} s^{-1}), and T is the ambient

https://doi.org/10.1021/acs.est.3c09122
Environ. Sci. Technol. 2024, 58, 5430−5441

Table 1. Temperature Sensitivity Factors ($f_{i,t,g}(T_{t,g})$) of Evaporative AVOC Emissions Used in This Study[a]

sources	temperature sensitivity factor $f_{i,t,g}(T_{t,g})$
fugitive emissions from transportation[32]	$f_{i=1,t,g}(T_{t,g}) = \frac{\overline{T}_g}{T_{t,g}}\exp\left(\frac{1.6 \pm 0.5 \times 10^4}{\overline{T}_g} - \frac{1.6 \pm 0.5 \times 10^4}{T_{t,g}}\right)$
solvent use[37]	$f_{i=2,t,g}(T_{t,g}) = \sqrt{\frac{\overline{T}_g}{T_{t,g}}}\cdot\exp\left(\frac{4.9 \pm 1.0 \times 10^3}{\overline{T}_g} - \frac{4.9 \pm 1.0 \times 10^3}{T_{t,g}}\right)$
other nonsolvent-use industrial (NSI) activities[14]	$f_{i=3,t,g}(T_{t,g}) = \frac{0.1 \pm 0.01 \times T_{t,g} - 26.6 \pm 4.0}{0.1 \pm 0.01 \times \overline{T}_g - 26.6 \pm 4.0}$

[a]Temperatures are in units of K.

temperature (unit: K). A_1 (unit: kg m^{-2} s^{-1} K) and B_1 (unit: K) are empirical temperature-dependency parameters; B_1 is analogous to the ratio between the enthalpy and the specific gas constant ($\Delta H/R$) in the Clausius−Clapeyron equation.

The evaporative VOC emissions associated with solvent use often involve evaporation from large surface areas, such as a painted or coated surface. Huang et al.[33] derived the form of evaporative fluxes from such surfaces based on statistical physics:

$$E_2 = \frac{A_2}{\sqrt{T}}\exp\left(\frac{-B_2}{T}\right) \quad (2)$$

where E_2 is the evaporative VOC flux associated with solvent use (unit: kg m^{-2} s^{-1}). A_2 (unit: kg m^{-2} s^{-1} K$^{1/2}$) and B_2 (unit: K) are the temperature-dependency parameters.

For the evaporative VOC emissions from NSI activities, there have not been systematic measurements of their temperature dependencies. Song et al.[14] used a positive matrix factorization (PMF) model to quantitatively attribute their observed ambient VOC concentrations in an industrial city to different sources. We adopted their observed linear temperature dependence for the ambient VOC concentrations associated with NSI activities (eq 3):

$$E_3 = A_3 T + B_3 \quad (3)$$

where E_3 is the evaporative VOC emission from NSI activities (unit: kg m^{-2} s^{-1}). A_3 (unit: kg m^{-2} s^{-1} K^{-1}) and B_3 (unit: kg m^{-2} s^{-1}) are empirically derived parameters.

We further assumed that the monthly mean AVOC emissions used in the BASE simulation represented the emission fluxes for the monthly mean temperature ($\overline{T}_g$) of the model grid g. Given the temperature dependence forms of eqs 1−3, we derived the temperature sensitivity factor of evaporative AVOC emissions, $f_{i,t,g}(T_{t,g})$, which described the ratio of AVOC flux from source i (see Table 1) at given temperature $T_{t,g}$, relative to the AVOC flux at monthly mean temperature $\overline{T}_g$ (eqs 4a−4c):

$$f_{i=1,t,g}(T_{t,g}) = \frac{\overline{T}_g}{T_{t,g}} \times \exp\left(\frac{B_1}{\overline{T}_g} - \frac{B_1}{T_{t,g}}\right) \quad (4a)$$

$$f_{i=2,t,g}(T_{t,g}) = \sqrt{\frac{\overline{T}_g}{T_{t,g}}}\cdot\exp\left(\frac{B_2}{\overline{T}_g} - \frac{B_2}{T_{t,g}}\right) \quad (4b)$$

$$f_{i=3,t,g}(T_{t,g}) = \frac{A_3 T_{t,g} + B_3}{A_3 \overline{T}_g + B_3} \quad (4c)$$

where i represents the different sources (i = 1 for transportation; i = 2 for solvent use; i = 3 for NSI activities). A_1 and A_2 from eqs 1 and 2 are eliminated. The parameter values in eqs 4a and 4c can be determined empirically to represent the emissions associated with the prevailing technology of source i. We reviewed the literature and selected parameter values most representative of Chinese conditions in 2017 (Table 1). We adopted the empirical value of B_1 and its uncertainty ($1.6 \pm 0.5 \times 10^4$ K) for China V standard light-duty gasoline car, which accounted for 87%[36] of the total number of vehicles in China in 2015.[32] For evaporative emissions from solvent use, we applied the experimental value of B_2 ($4.9 \pm 1.0 \times 10^3$ K) for formaldehyde,[37] whose emission from building materials had a temperature dependency similar to that of other common solvents.[38] A_3 (0.1 ± 0.01 kg m^{-2} s^{-1} K^{-1}) and B_3 (26.6 ± 4.0 kg m^{-2} s^{-1}) and their uncertainty ranges were fitted from Song et al.[14] based on measurements in a Northern Chinese city in 2017.

The temperature sensitivity factors were applied to the AVOC(T) simulation to represent the variation of AVOC emissions as perturbed by hourly ambient temperatures (eq 5):

$$E_{i,j,t,g} = c_{i,j,g}\left[f_{i,t,g}(T_{t,g})\cdot\gamma_i + (1 - \gamma_i)\right]E_{0,i,j,t,g} \quad (5)$$

where $E_{i,j,t,g}$ is the emission rate of AVOC species j from source i for model grid g at time t. $E_{0,i,j,t,g}$ are the temperature-independent emission rates of species j in the BASE simulation. $T_{t,g}$ is the surface air temperature for model grid g at time t, and $f_{i,t,g}(T_{t,g})$ is the corresponding temperature sensitivity factor for source i. We defined γ_i as the evaporable (i.e., ambient-temperature-sensitive) fraction of AVOC emissions from source i, which was the fugitive fraction of AVOC emissions from that source.[39] Nonfugitive AVOC emissions, such as tailpipe exhaust from vehicles, are more affected by the temperature within engines and less affected by ambient temperature. For transportation emissions, we assumed γ_1 = 0.39 based on emission tests for Chinese passenger vehicles and trucks in the year 2015.[31] We assumed the same temperature sensitivity for both on-road and off-road vehicles because all vehicles could release evaporative AVOC emissions during hot soak loss, diurnal breathing loss, refueling loss, and running loss.[31] For AVOC emissions from solvent use (i = 2) and NSI activities (i = 3), we assumed γ_i = 1 because (1) the emissions associated with solvent use were mostly fugitive and (2) the temperature sensitivity factor we adopted for NSI emissions were from the observed variation of ambient VOC concentrations and accounted for the fugitive fraction implicitly. Finally, we applied a normalizing factor ($c_{i,j,g}$) to each model grid, such that, for species j, the sum of emissions

https://doi.org/10.1021/acs.est.3c09122
Environ. Sci. Technol. 2024, 58, 5430−5441

from source i during the simulation period in the AVOC(T) simulation ($\sum_t E_{i,j,t,g}$) was identical to the sum of emissions from that source in the BASE simulation ($\sum_t E_{0,i,j,t,g}$) (Figure S2). This normalization ensured that the simulated differences in surface ozone were driven only by the temperature-induced variability of evaporative AVOC emissions.

2.3. Calculation of OFP Driven by the Temperature Sensitivity of VOC. The OFP is a widely used metric to quantify the total photochemical production of ozone from individual VOC species throughout its entire photochemical cascade.[40] For unit emission of a VOC species j released into a boundary layer box of known volume, its OFP is the product of its emission and its emission-based maximum increment reactivity (MIR_j; unit: g O_3 g^{-1} VOC).[9,41,42] Assuming that the local photochemical conditions (e.g., oxidant levels, actinic fluxes) were unchanged, the local change of OFP of species j at model grid g at time t ($\Delta OFP_{i,j,t,g}$; unit: g of O_3) would be proportional to the local change of its emission $\Delta E_{i,j,t,g}$ (unit: g of VOC s^{-1}):

$$\Delta OFP_{i,j,t,g} = \Delta E_{i,j,t,g} \times MIR_j \quad (6)$$

We adopted the MIR_j values calculated for Chinese cities from previous studies.[43−45]

2.4. Surface Observations of Ozone Concentrations and Meteorological Conditions, and Satellite Observations of Tropospheric NO_2 and Formaldehyde Column Concentrations. We compared model results to hourly measurements of surface ozone concentrations at 91 sites in 13 cities in the BTH area during summer 2017. The measurements were managed by the National Environmental Monitoring Centre (http://www.cnemc.cn, last accessed: March 30, 2023). We applied a consistent data quality control protocol[1,5] to the hourly measurements and averaged them onto the model grids for comparison with the simulations. We used the hourly meteorological data downloaded from the National Centers for Environmental Information (NCEI, http://www.ncdc.noaa.gov, last accessed: January 10, 2024) to evaluate the simulated meteorology.

Satellite-observed formaldehyde-to-NO_2 column concentration ratios (FNR) have been used as a qualitative indicator for the regional ozone photochemical regime.[46−48] We used the Level 3 Cloud-Screened Tropospheric Column NO_2 product (0.25° resolution)[49] and the Total Column Daily Level 3 Weighted Mean Global HCHO product (0.1° resolution)[50] from the Ozone Monitoring Instrument (OMI, nadir overpass time at approximately 13:45 local time) to calculate observed FNR over the BTH area in summer 2017. Both datasets were interpolated to 0.25° resolution for our analysis.

3. RESULTS

3.1. Evaluation of Surface Ozone Concentrations Simulated by the BASE Experiment. We first evaluated WRF-GC's performance in simulating the observed meteorological conditions and surface ozone concentrations between June 1 and July 5, 2017. The WRF-GC simulations, nudged with NCEP reanalysis data, reproduced the spatiotemporal variability of observed surface temperature and relative humidity (Figures S3 and S4). The BASE simulation reproduced the spatial distribution of MDA8 ozone concentrations over the BTH area (Figure S5, spatial correlation r = 0.64). The simulated MDA8 ozone concentration over the BTH area during this period averaged 179 ± 40 $\mu g\ m^{-3}$, in good agreement with the observations in terms of mean (160 ± 38 $\mu g\ m^{-3}$) and variability (Figure S6, temporal correlation r = 0.79). Observed BTH-mean MDA8 ozone concentrations exceeded the national air quality standard of 160 $\mu g\ m^{-3}$ during June 14−21 (hereafter referred to as Episode 1) and from June 25 to July 5 (Episode 2). The BASE simulation correctly simulated 17 of these 19 ozone exceedance days in the BTH area (Figure S6), which formed the basis for our subsequent analyses. However, the model tended to underestimate ozone levels on exceedance days and the midday ozone concentrations (Figure S6), potentially reflecting a subdued sensitivity of ozone to temperature in the BASE simulation.

3.2. Simulated Temperature Dependencies of Regional Anthropogenic and Biogenic VOC Emissions. Figure 1 shows $[\gamma_i \cdot f_{i,t,g}(T_{t,g}) + (1 - \gamma_i)]$ from eq 5, which was

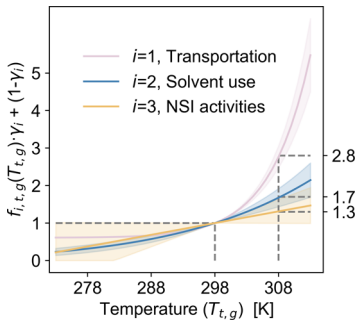

Figure 1. Effective temperature sensitivity of total AVOC emissions from transportation (i = 1, light purple), solvent use (i = 2, blue), and NSI activities (i = 3, yellow) for a model grid g at time t, relative to the monthly mean temperature of $\overline{T}_g$ = 298 K for that grid. The gray dashed lines mark the ratios of AVOC emissions at 308 K relative to their emissions at 298 K. The shaded areas represent the ranges of uncertainty associated with the empirical parameters in eqs 4a−4c.

our parametrized effective temperature sensitivity of the total (evaporative and nonevaporative) AVOC flux from source i, assuming a monthly mean temperature $\overline{T}_g$ of 298 K at model grid g. The shaded areas represent the ranges of uncertainty associated with the empirical parameters used in eqs 4a−4c. The AVOC emissions from transportation grew only weakly with temperature below $\overline{T}_g$ but increased sharply with temperature above $\overline{T}_g$. At 10 K above $\overline{T}_g$, the AVOC flux from transportation was 2.8 times its flux at $\overline{T}_g$. In contrast, the AVOC fluxes associated with solvent use and NSI activities increased roughly linearly with temperature. At 10 K above $\overline{T}_g$, the AVOC fluxes from solvent use and NSI activities were 1.7 and 1.3 times their respective fluxes at $\overline{T}_g$. The AVOC species from transportation and solvent-use emissions consisted of high fractions of alkenes and aromatics of high OFPs. We thus hypothesized that the temperature sensitivity of the AVOC emissions from transportation and solvent use may substantially aggravate surface ozone pollution during anomalously warm weather.

Figure 2a shows the daily variations of BTH-averaged AVOC and BVOC emissions in response to daily temperature variations, as simulated by our WRF-GC sensitivity experiments. During the study period, the daily mean temperature over the BTH area varied between 291 and 304 K. In particular, the pollution Episodes 1 and 2 both corresponded to periods of anomalously warm temperatures. Daily temperature variations caused the BTH-wide daily AVOC emissions

https://doi.org/10.1021/acs.est.3c09122
Environ. Sci. Technol. 2024, 58, 5430−5441

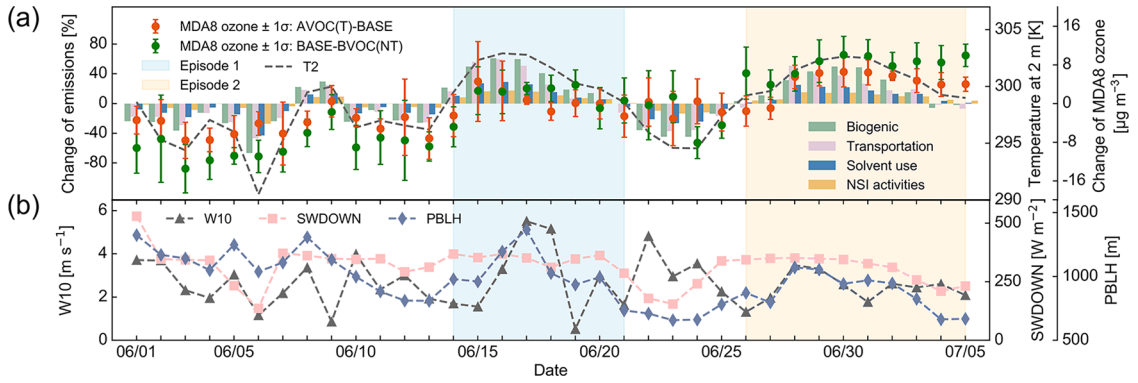

Figure 2. (a) Time series of simulated daily surface air temperature (T2, gray dashed line), daily variations of BTH-mean VOC emissions from anthropogenic and biogenic sources relative to their respective monthly means (bars), and the simulated MDA8 ozone responses to temperature-dependent anthropogenic (red dots and whiskers) and biogenic (green dots and whiskers) VOC emissions. (b) Time series of simulated 10 m wind speeds (W10, gray dashed line with triangles), downward shortwave radiation fluxes (SWDOWN, pink dashed line with squares), and planetary boundary layer height (PBLH, blue dashed line with diamonds) over the BTH area during the simulation period. The time periods of two ozone exceedance episodes are shaded in blue (Episode 1) and yellow (Episode 2).

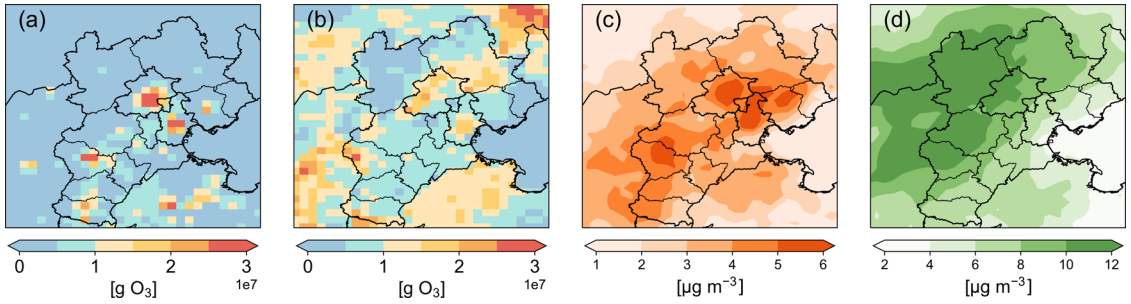

Figure 3. Spatial distributions of mean OFP enhancements (unit: g of O_3) driven by temperature-dependent (a) AVOC and (b) BVOC emissions during Episode 2. Also shown are the spatial distributions of simulated mean MDA8 ozone enhancements (unit: $\mu g\ m^{-3}$) driven by temperature-dependent (c) AVOC and (d) BVOC emissions.

from the three anthropogenic sectors to vary substantially by −39 to 35% relative to their respective monthly means. For the entire BTH area, the temporal correlations between the BTH-mean daily temperature and BTH-wide AVOC emissions from the three sectors were 0.92, 0.97, and 0.98, respectively. The overall sensitivity of total (from all sectors) AVOC emissions to temperature was 6.25% K^{-1} over the BTH during the simulated period. Transportation AVOC emissions contributed the most to this overall temperature sensitivity (9.7% K^{-1}), especially on warm days. Solvent use and NSI activities contributed 5.8 and 3.4% K^{-1}, respectively, to the overall temperature sensitivity of the total AVOC emissions. In comparison, daily temperature variations drove daily BVOC emission variability between −67 and 61%, resulting in a temperature sensitivity of 11.2% K^{-1} and temporal correlation against a daily temperature $r = 0.97$. In short, the temperature sensitivity of total AVOC emissions was comparable in magnitude to the temperature sensitivity of BVOC on a BTH-wide regional scale.

3.3. Simulated Responses of Surface Ozone to Temperature-Dependent VOC Emissions. Figure 2a also shows the responses of BTH MDA8 ozone to the temperature-dependent AVOC and BVOC emissions, represented by the simulated ozone differences between the AVOC(T) and the BASE experiments and by the differences between the BASE and the BVOC(NT) experiments, respectively. The monthly mean MDA8 ozone over the BTH area in the AVOC(T) (159 ± 42 $\mu g\ m^{-3}$) and BVOC(NT) (161 ± 32 $\mu g\ m^{-3}$) simulations were similar to that in the BASE simulation (160 ± 38 $\mu g\ m^{-3}$) because we constrained the monthly mean VOC emissions to be the same in all simulations. The nonlinear impacts on the simulated ozone differences were small because in all simulations: (1) the OH concentrations were relatively similar (less than 10% difference, Figure S7a), (2) the ozone production in most of the BTH cities was NO_x-saturated (discussed in Section 3.4), and (3) RO_2 was mainly produced by the photolysis of oxygenated products of AVOCs and BVOCs. The inclusion of AVOC's temperature dependence enhanced the daily variability of ozone, as shown by the −7.6 $\mu g\ m^{-3}$ (June 3) to 6.6 $\mu g\ m^{-3}$ (June 30) difference relative to the BASE simulation (Figure 2a), and this inclusion also slightly improved the temporal correlation of daily simulated MDA8 ozone concentrations with the observations in 9 of 13 cities in the BTH area (Figure S8). We found that the daily ozone variability induced by the AVOC−temperature relationship was comparable to the daily ozone variability induced by the BVOC−temperature relationship (−13.5 $\mu g\ m^{-3}$ on June 3 to 10.1 $\mu g\ m^{-3}$ June 30; Figure 2a). Temperature-enhanced AVOC and BVOC emissions both contributed to exacerbating ozone exceedances during the warm periods of Episodes 1 and 2. During the cool period between June 3 and 8, both AVOC and BVOC emissions were subdued, resulting in comparable contributions to the decreased surface ozone concentrations.

The responses of surface ozone to temperature-enhanced VOC emissions were also modulated by other meteorological variables (Figure 2b), reflecting the complex meteorological

https://doi.org/10.1021/acs.est.3c09122
Environ. Sci. Technol. 2024, 58, 5430−5441

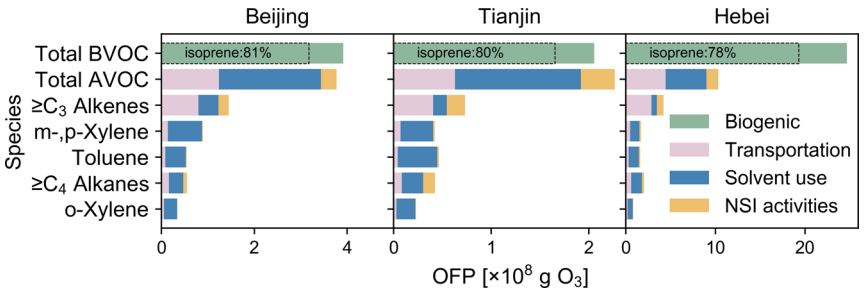

Figure 4. OFP enhancements driven by temperature-dependent VOC emissions over Beijing (left), Tianjin (middle), and Hebei (right) during Episode 2. The source sectors are color-coded. The OFP enhancements from the top five contributing AVOC species are also shown. The OFP for each city/province is the sum of the episode-averaged OFP for all grids within that city/province.

control of pollutant emissions, advection, accumulation, and photochemistry. During the warm period of Episode 2, the daily maximum temperature over the BTH was 3.5 K above the monthly mean, and the MDA8 ozone enhancements due to temperature-dependent AVOC and BVOC emissions were 6.1 and 8.5 μg m^{-3}, respectively. Episode 2 was marked by strong downward shortwave radiation flux (>340 W m^{-2}), low surface wind speeds (<3 m s^{-1}), and relatively low planetary boundary layer heights (<1000 m), all of which were favorable conditions for the accumulation of ozone precursors and their local photochemical production of ozone.[51,52] In contrast, during Episode 1, the response of MDA8 ozone to temperature-enhanced VOC was slightly subdued partly because the high temperatures lasted shorter than they did during Episode 2. Additionally, the high planetary boundary layer heights (12% above the monthly mean) and enhanced surface winds (19% above the monthly mean) during Episode 1 promoted the dispersion of ozone and its precursors such that the impacts of temperature-enhanced anthropogenic and biogenic VOC emissions on local ozone production were both diminished.

We further analyzed how temperature-dependent VOC emissions from different sectors contributed to surface ozone pollution during Episode 2. Figure 3 shows the spatial distributions of the OFP enhancements during Episode 2 driven by temperature-dependent AVOC and BVOC emissions, respectively. The OFP enhancements associated with increased AVOC emissions were highest over Beijing, Tianjin, Tangshan, and Baoding (Figure S9). The simulated ozone enhancements associated with increased AVOCs were spatially consistent with the corresponding OFP enhancements, with the largest ozone enhancements exceeding 6 μg m^{-3} over the four aforementioned cities (Figure 3a,c). In contrast, the OFP enhancements associated with temperature-dependent BVOC emissions were spatially correlated with increased isoprene emissions (Figures 3b and S5b), but the simulated ozone enhancements were slightly displaced northwest of the BTH area (Figures 3d and S5b). This displacement was because the oxidation of isoprene first produced its intermediate products, such as methacrolein and methyl vinyl ketone, formaldehyde, and acetaldehyde, which in turn photochemically form ozone.[53] All of these intermediate products have lifetimes ranging from a few hours to a day, which were longer than those of isoprene. As a result, these products were transported downwind by the surface easterly and southerly winds (Figure S10), and the eventual ozone formation was spatially displaced and lagged behind the initial oxidation of isoprene for several hours. In contrast, the photochemical production of ozone from highly reactive alkenes (e.g., propene) and aromatics (e.g., *m*-xylenes) began immediately after the initial oxidation of these precursors.[54] This difference in the ozone production time scales from reactive AVOCs and from isoprene is consistent with evidence from chamber experiments. Compared to BVOCs, temperature-dependent AVOC emissions have a more localized impact on surface ozone. In the WRF-GC model and for our simulation period, the inclusion of temperature-sensitive AVOC emissions led to less than 10% perturbation on the regional OH levels (Figure S7a); the difference in the simulated biogenic secondary organic aerosol abundance was also small (Figure S11).

Figure 4 compares the temperature-induced OFP enhancements contributed by different AVOC and BVOC species and sectors over Beijing, Tianjin, and Hebei, respectively, during Episode 2. The temperature dependencies of BVOCs and AVOCs contributed comparably to the OFP enhancements over Beijing and Tianjin, but BVOCs contributed twice as much OFP enhancements than AVOCs over Hebei. Averaged over the three cities and provinces, the temperature-enhanced OFP associated with AVOCs was mostly associated with transportation (50%) and solvent-use (40%) emissions, with only minor contributions from NSI activities (10%), confirming our hypothesis. In terms of chemical species, short-lived aromatics (including toluene and xylenes, mostly from solvent-use emissions) were the largest contributors (45%) to the anthropogenic OFP enhancements, followed by ≥C_3 alkenes (largely from transportation) and ≥C_4 alkenes (from both transportation and solvent-use emissions). These results indicated that over areas with strong AVOC emissions, selectively reducing the evaporative emissions of highly reactive species from transportation and solvent use would mitigate the local ozone pollution associated with warm temperatures.

3.4. Ozone−Temperature Relationship as Driven by Temperature-Dependent VOC Emissions. We analyzed whether and how the inclusion of temperature-dependent AVOC emissions improved the representation of the ambient ozone−meteorology relationship in the model. Figure S12 shows the simulated MDA8 ozone enhancements ($\Delta MDA8O_3$) driven by temperature-dependent AVOC and BVOC emissions, respectively, as a function of mean afternoon (13:00−17:00) temperature anomaly (ΔT) for cities in the BTH area and for the BTH as a whole. We defined the ozone-temperature sensitivity (k) as the slope of the reduced-major axis regression line of $\Delta MDA8O_3$ versus ΔT. The temperature dependency of AVOC emissions drove simulated ozone-temperature sensitivities (k_A) of 1.0 to 1.8 μg m^{-3} K^{-1}, which were on average 70% of the total simulated ozone-temperature

https://doi.org/10.1021/acs.est.3c09122
Environ. Sci. Technol. 2024, 58, 5430−5441

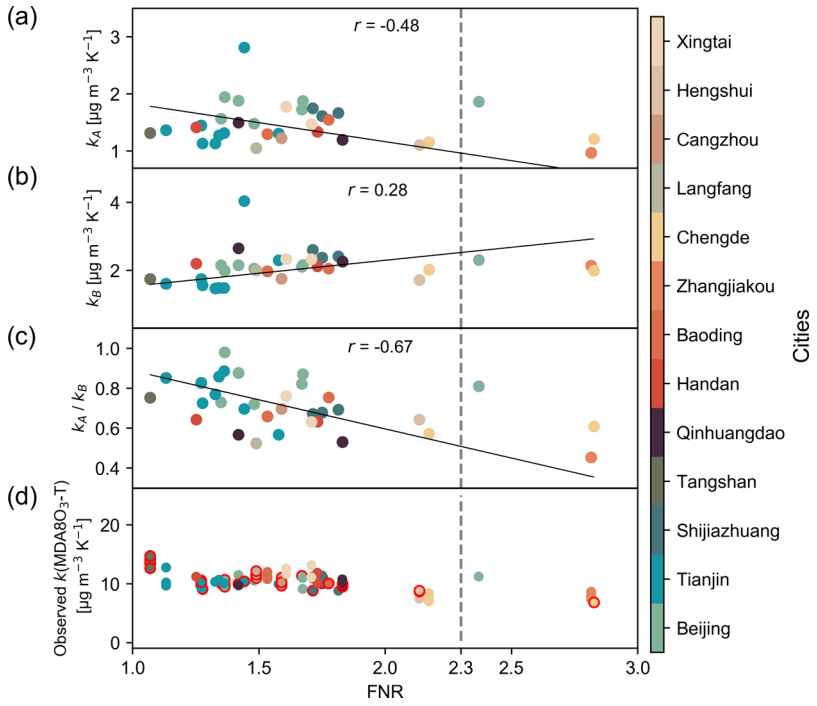

Figure 5. Simulated ozone-temperature sensitivities for each city in the BTH area as driven by temperature-enhanced (a) AVOC emissions (k_A) and (b) BVOC emissions (k_B), and (c) the ratio of k_A/k_B versus the FNR values observed by the OMI. Also shown are (d) observed ozone-temperature sensitivity for each city (observed MDA8 ozone anomaly versus afternoon (13:00−17:00) temperature anomaly during ozone episodes). The symbols are outlined in red if the inclusion of temperature-enhanced evaporative AVOC emissions in the model improved the simulated overall ozone-temperature sensitivity on ozone exceedance days. The gray dashed line represents the threshold between a NO_x-saturated (VOC-sensitive) regime and a transition regime for ozone photochemical production.

sensitivity driven by the temperature dependency of BVOCs emissions (k_B = 1.7−2.4 μg m^{-3} K^{-1}).

We investigated whether the variable values of k_A and k_B across BTH cities may be related to the local ozone production regimes in each city. Our simulated FNRs from the AVOC(T) experiment were spatially consistent with the OMI-observed FNRs (Figure S13), indicating that the model reproduced the spatial difference of the ozone production regimes over the BTH area. Furthermore, we found that in our simulations both the FNR and the H_2O_2/HNO_3 ratios[55] were not significantly different in the BASE and AVOC(T) experiments, indicating that the regime of ozone production was not substantially altered by the inclusion of temperature-sensitive AVOC emissions (Figure S7b). Figure 5 shows the simulated values of k_A and k_B and their ratios versus the OMI-observed FNR values over model grids with surface ozone measurements during the study period. Previous model studies over East China have shown that FNR < 2.3 and FNR > 4.2, respectively, indicated local ozone production to be NO_x-saturated (or VOC-sensitive) and NO_x-sensitive, while an FNR value between 2.3 and 4.2 indicated ozone production to be in a transitional regime.[56] Based on these thresholds, ozone production in most of the 13 cities in the BTH area was VOC-sensitive (Figure 5). The k_B values across BTH cities were not significantly correlated with FNR, which may be due in part to the delayed ozone production from isoprene oxidation (discussed in Section 3.3). However, k_A values (r = −0.48, two-tail p-value <0.005) and k_A/k_B values (r = −0.67, two-tail p-value <10^{-4}) across BTH cities were negatively correlated with FNRs. These negative correlations indicated that in cities where ozone production was severely saturated with NO_x emissions and thus highly sensitive to VOC emissions, the localized production of ozone from temperature-dependent AVOC emissions would contribute more substantially to the overall ozone−temperature relationship, compared to the cities with FNR > 2.3, such as Zhangjiakou and Chengde (Figures 5 and S13). In these latter cities, ozone production was in the transitional regime and less sensitive to increased VOC emissions; as such, both k_A and k_A/k_B were relatively small in Zhangjiakou and Chengde (Figure 5).

The observed surface ozone-temperature sensitivity over the BTH cities on ozone exceedance (MDA8 ozone > 160 μg m^{-3}) days (9.8 ± 2 μg m^{-3} K^{-1}, Figure S14) were larger than the sum of k_A and k_B, indicating that there were other coupling mechanisms between temperature and ozone pollution at play, in addition to the temperature dependencies of AVOC and BVOC emissions explored in this study. These other coupling mechanisms may include the actinic flux-dependency of BVOC emissions, the temperature-dependency of soil NO_x emissions, surface stagnation and boundary layer compression associated with subsidence and anticyclonic weather, advection of ozone from other parts of Eastern China, and faster photochemical reactions and less ozone removal under warm and dry weather.[5,7,57,58] Nevertheless, the inclusion of the temperature-dependent AVOC emissions in our model improved the simulated ozone-temperature sensitivities (from 8.3 ± 1 μg m^{-3} K^{-1} in the BASE experiment to 9.5 ± 1 μg m^{-3} K^{-1} in the AVOC(T) experiment) over the BTH area as a whole and at most BTH cities on ozone exceedance days (Figures 5d).

4. UNCERTAINTIES AND IMPLICATIONS FOR REGIONAL AIR QUALITY MANAGEMENT

Our parametrizations for the temperature dependency of evaporative AVOC emissions involve uncertainties arising from

https://doi.org/10.1021/acs.est.3c09122
Environ. Sci. Technol. 2024, 58, 5430−5441

several aspects, including the scarcity of observational constraints on the temperature dependence of individual sources and species, as well as the continued change of emission control policies in China. For example, we assumed the same temperature sensitivity for evaporative emissions from on-road and off-road vehicles, but the fuel types and emission regulations for these vehicles are in fact different.[24,59] For NSI emissions, our use of parameters derived from the source-apportionment study of Song et al.[14] may be sensitive to their measurements and apportionment techniques. In addition, the Chinese government has promulgated stronger control policies on AVOC emissions since 2021.[60] Emission standards for vehicles have also tightened,[61] and in many cities a significant portion of the on-road fleet has become electrical.[62] These changes likely have substantial impacts on the evaporative AVOC emissions. However, measurements in 2021 showed that fugitive emissions still constituted more than half of the total VOC emissions from several industrial processes, including coating.[39] More measurements representative of current technologies are urgently needed to reduce the uncertainties of the parameters in Table 1 and better represent the temperature sensitivities of evaporative emissions of AVOC species from individual sources in China.

Application of our parametrizations in regional models can help improve air quality forecasts and accentuate targets for emission reduction, providing policymakers with effective guidance in air quality management. A persistent issue in current air quality models is the tendency to underestimate high ozone pollution events.[63,64] We demonstrated that incorporating the temperature-dependency of evaporative AVOC emissions into the model helps rectify this underestimation by improving the simulated ozone-temperature sensitivity, especially in major cities. Our findings also highlighted the need to strengthen the control of evaporative emissions of high-reactivity AVOC species, including higher alkenes and aromatics, which is already an emission reduction priority set by the Chinese Ministry of Ecology and Environment.[65] Furthermore, reducing evaporative AVOC emissions on hot days, such as temporarily suspending vehicular and industrial refueling, open-air painting, and asphalt laying, may be viable emergency response measures to mitigate ozone exceedance episodes in urban areas.

Our results also highlighted a previously underexplored factor in the "climate change penalty" of surface ozone pollution, which is the deterioration of ozone air quality as a result of climate warming even when anthropogenic activities remain unchanged. Studies have shown that global warming may increase the frequency and intensities of heatwaves and urban heat island effects,[7,66] such that the impacts of temperature-dependent AVOC emissions on ozone may become more pronounced in the future. Other underestimated or unrepresented natural and anthropogenic emissions of ozone precursors, such as soil-NO_x emissions[67] and emissions associated with urban greening practices,[68−70] may also cause complex ozone-temperature sensitivities. These linkages between air pollution and meteorology should be considered in our projection of long-term air quality trends to better inform the long-term emission reduction goals.

■ ASSOCIATED CONTENT

Supporting Information

The Supporting Information is available free of charge at https://pubs.acs.org/doi/10.1021/acs.est.3c09122.

Simulation setup, evaluations of simulated meteorology and ozone concentrations against observations, differences of simulated ozone production regime indicators between the experiments, simulated biogenic secondary organic aerosols, and simulated ozone-temperature sensitivities (PDF)

■ AUTHOR INFORMATION

Corresponding Authors

Tzung-May Fu − *Shenzhen Key Laboratory of Precision Measurement and Early Warning Technology for Urban Environmental Health Risks, School of Environmental Science and Engineering and Guangdong Provincial Observation and Research Station for Coastal Atmosphere and Climate of the Greater Bay Area, School of Environmental Science and Engineering, Southern University of Science and Technology, Shenzhen, Guangdong 518055, China;* orcid.org/0000-0002-8556-7326; Email: fuzm@sustech.edu.cn

Steve R. Arnold − *Institute for Climate and Atmospheric Science, School of Earth and Environment, University of Leeds, Leeds LS2 9JT, U.K.;* orcid.org/0000-0002-4881-5685; Email: s.arnold@leeds.ac.uk

Authors

Wenlu Wu − *Shenzhen Key Laboratory of Precision Measurement and Early Warning Technology for Urban Environmental Health Risks, School of Environmental Science and Engineering and Guangdong Provincial Observation and Research Station for Coastal Atmosphere and Climate of the Greater Bay Area, School of Environmental Science and Engineering, Southern University of Science and Technology, Shenzhen, Guangdong 518055, China; Institute for Climate and Atmospheric Science, School of Earth and Environment, University of Leeds, Leeds LS2 9JT, U.K.;* orcid.org/0009-0005-0901-7217

Dominick V. Spracklen − *Institute for Climate and Atmospheric Science, School of Earth and Environment, University of Leeds, Leeds LS2 9JT, U.K.*

Aoxing Zhang − *Shenzhen Key Laboratory of Precision Measurement and Early Warning Technology for Urban Environmental Health Risks, School of Environmental Science and Engineering and Guangdong Provincial Observation and Research Station for Coastal Atmosphere and Climate of the Greater Bay Area, School of Environmental Science and Engineering, Southern University of Science and Technology, Shenzhen, Guangdong 518055, China;* orcid.org/0000-0002-0716-5452

Wei Tao − *Shenzhen Key Laboratory of Precision Measurement and Early Warning Technology for Urban Environmental Health Risks, School of Environmental Science and Engineering and Guangdong Provincial Observation and Research Station for Coastal Atmosphere and Climate of the Greater Bay Area, School of Environmental Science and Engineering, Southern University of Science and Technology, Shenzhen, Guangdong 518055, China*

Xiaolin Wang − *John A. Paulson School of Engineering and Applied Sciences, Harvard University, Cambridge, Massachusetts 02138, United States*

Yue Hou − *Shenzhen Key Laboratory of Precision Measurement and Early Warning Technology for Urban Environmental Health Risks, School of Environmental Science and Engineering and Guangdong Provincial Observation and Research Station for Coastal Atmosphere and Climate of the*

https://doi.org/10.1021/acs.est.3c09122
Environ. Sci. Technol. 2024, 58, 5430−5441

Greater Bay Area, School of Environmental Science and Engineering, Southern University of Science and Technology, Shenzhen, Guangdong 518055, China

Jiajia Mo − *Shenzhen Key Laboratory of Precision Measurement and Early Warning Technology for Urban Environmental Health Risks, School of Environmental Science and Engineering and Guangdong Provincial Observation and Research Station for Coastal Atmosphere and Climate of the Greater Bay Area, School of Environmental Science and Engineering, Southern University of Science and Technology, Shenzhen, Guangdong 518055, China*

Jiongkai Chen − *Shenzhen Key Laboratory of Precision Measurement and Early Warning Technology for Urban Environmental Health Risks, School of Environmental Science and Engineering and Guangdong Provincial Observation and Research Station for Coastal Atmosphere and Climate of the Greater Bay Area, School of Environmental Science and Engineering, Southern University of Science and Technology, Shenzhen, Guangdong 518055, China;* orcid.org/0000-0001-9545-3333

Yumin Li − *Shenzhen Key Laboratory of Precision Measurement and Early Warning Technology for Urban Environmental Health Risks, School of Environmental Science and Engineering and Guangdong Provincial Observation and Research Station for Coastal Atmosphere and Climate of the Greater Bay Area, School of Environmental Science and Engineering, Southern University of Science and Technology, Shenzhen, Guangdong 518055, China*

Xu Feng − *John A. Paulson School of Engineering and Applied Sciences, Harvard University, Cambridge, Massachusetts 02138, United States;* orcid.org/0000-0002-8226-9403

Haipeng Lin − *John A. Paulson School of Engineering and Applied Sciences, Harvard University, Cambridge, Massachusetts 02138, United States*

Zhijiong Huang − *Institute for Environmental and Climate Research, Jinan University, Guangzhou, Guangdong 511443, China*

Junyu Zheng − *Sustainable Energy and Environment Thrust, The Hong Kong University of Science and Technology (Guangzhou), Guangzhou, Guangdong 511453, China;* orcid.org/0000-0002-8267-7255

Huizhong Shen − *Shenzhen Key Laboratory of Precision Measurement and Early Warning Technology for Urban Environmental Health Risks, School of Environmental Science and Engineering and Guangdong Provincial Observation and Research Station for Coastal Atmosphere and Climate of the Greater Bay Area, School of Environmental Science and Engineering, Southern University of Science and Technology, Shenzhen, Guangdong 518055, China;* orcid.org/0000-0003-1335-8477

Lei Zhu − *Shenzhen Key Laboratory of Precision Measurement and Early Warning Technology for Urban Environmental Health Risks, School of Environmental Science and Engineering and Guangdong Provincial Observation and Research Station for Coastal Atmosphere and Climate of the Greater Bay Area, School of Environmental Science and Engineering, Southern University of Science and Technology, Shenzhen, Guangdong 518055, China*

Chen Wang − *Shenzhen Key Laboratory of Precision Measurement and Early Warning Technology for Urban Environmental Health Risks, School of Environmental Science and Engineering and Guangdong Provincial Observation and Research Station for Coastal Atmosphere and Climate of the Greater Bay Area, School of Environmental Science and Engineering, Southern University of Science and Technology, Shenzhen, Guangdong 518055, China;* orcid.org/0000-0001-9565-8777

Jianhuai Ye − *Shenzhen Key Laboratory of Precision Measurement and Early Warning Technology for Urban Environmental Health Risks, School of Environmental Science and Engineering and Guangdong Provincial Observation and Research Station for Coastal Atmosphere and Climate of the Greater Bay Area, School of Environmental Science and Engineering, Southern University of Science and Technology, Shenzhen, Guangdong 518055, China*

Xin Yang − *Shenzhen Key Laboratory of Precision Measurement and Early Warning Technology for Urban Environmental Health Risks, School of Environmental Science and Engineering and Guangdong Provincial Observation and Research Station for Coastal Atmosphere and Climate of the Greater Bay Area, School of Environmental Science and Engineering, Southern University of Science and Technology, Shenzhen, Guangdong 518055, China;* orcid.org/0000-0002-9173-1188

Complete contact information is available at: https://pubs.acs.org/10.1021/acs.est.3c09122

Author Contributions

W.W., T.F., S.A., and D.S. designed the study. W.W. carried out the WRF-GC experiments. A.Z., W.T., X.W., Y.H., J.M.J.C., X.F., and H.L. developed the WRF-GC simulations. W.W. analyzed the results. W.W. and T.F. wrote the manuscript. All authors contributed to the manuscript.

Funding

This work was supported by the National Natural Science Foundation of China (42325504, 42011530176), the Shenzhen Key Laboratory of Precision Measurement and Early Warning Technology for Urban Environmental Health Risks (ZDSYS20220606100604008), the Shenzhen Science and Technology Program (KQTD20210811090048025, JCYJ20220818100611024), the Guangdong Basic and Applied Basic Research Foundation (2020B1515130003, 2021A1515110748), the Guangdong University Research Project Science Team (2021KCXTD004), and the Guangdong Province Major Talent Program (2019CX01S188).

Notes

The authors declare no competing financial interest.

■ ACKNOWLEDGMENTS

This work was supported by the National Natural Science Foundation of China (42325504, 42011530176), the Shenzhen Key Laboratory of Precision Measurement and Early Warning Technology for Urban Environmental Health Risks (ZDSYS20220606100604008), the Shenzhen Science and Technology Program (KQTD20210811090048025, JCYJ20220818100611024), the Guangdong Basic and Applied Basic Research Foundation (2020B1515130003, 2021A1515110748), the Guangdong University Research Project Science Team (2021KCXTD004), and the Guangdong Province Major Talent Program (2019CX01S188). Computational resources were supported by the Center for Computational Science and Engineering at the Southern University of Science and Technology.

REFERENCES

(1) Lu, X.; Hong, J. Y.; Zhang, L.; Cooper, O. R.; Schultz, M. G.; Xu, X. B.; Wang, T.; Gao, M.; Zhao, Y. H.; Zhang, Y. H. Severe surface ozone pollution in China: A global perspective. *Environmental Science & Technology Letters* **2018**, *5* (8), 487−494.

(2) Silver, B.; Reddington, C. L.; Arnold, S. R.; Spracklen, D. V. Substantial changes in air pollution across China during 2015−2017. *Environmental Research Letters* **2018**, *13* (11), No. 114012.

(3) Ministry of Environmental Protection of the People's Republic of China (MEP). *2013 Report on the State of the Ecology and Environment in China*; 2014. https://www.mee.gov.cn/hjzl/sthjzk/zghjzkgb/201605/P020160526564151497131.pdf (accessed February 2023).

(4) Ministry of Ecology and Environment of People's Republic of China (MEE). *2019 Report on the State of the Ecology and Environment in China*; 2020. https://www.mee.gov.cn/hjzl/sthjzk/zghjzkgb/202006/P020200602509464172096.pdf (accessed February 2023).

(5) Wang, X. L.; Fu, T. M.; Zhang, L.; Cao, H. S.; Zhang, Q.; Ma, H. C.; Shen, L.; Evans, M. J.; Ivatt, P. D.; Lu, X.; Chen, Y. F.; Zhang, L. J.; Feng, X.; Yang, X.; Zhu, L.; Henze, D. K. Sensitivities of ozone air pollution in the Beijing-Tianjin-Hebei area to local and upwind precursor emissions using adjoint modeling. *Environ. Sci. Technol.* **2021**, *55* (9), 5752−5762.

(6) Guenther, A. B.; Jiang, X.; Heald, C. L.; Sakulyanontvittaya, T.; Duhl, T.; Emmons, L. K.; Wang, X. The Model of Emissions of Gases and Aerosols from Nature version 2.1 (MEGAN2.1): An extended and updated framework for modeling biogenic emissions. *Geoscientific Model Development* **2012**, *5* (6), 1471−1492.

(7) Fu, T. M.; Tian, H. Climate change penalty to ozone air quality: Review of current understandings and knowledge gaps. *Current Pollution Reports* **2019**, *5* (3), 159−171.

(8) Cetin, E.; Odabasi, M.; Seyfioglu, R. Ambient volatile organic compound (VOC) concentrations around a petrochemical complex and a petroleum refinery. *Sci. Total Environ.* **2003**, *312* (1−3), 103−112.

(9) Li, M.; Zhang, Q.; Zheng, B.; Tong, D.; Lei, Y.; Liu, F.; Hong, C. P.; Kang, S. C.; Yan, L.; Zhang, Y. X.; Bo, Y.; Su, H.; Cheng, Y. F.; He, K. B. Persistent growth of anthropogenic non-methane volatile organic compound (NMVOC) emissions in China during 1990−2017: Drivers, speciation and ozone formation potential. *Atmospheric Chemistry and Physics* **2019**, *19* (13), 8897−8913.

(10) Niu, Z. Z.; Kong, S. F.; Zheng, H.; Yan, Q.; Liu, J. H.; Feng, Y. K.; Wu, J.; Zheng, S. R.; Zeng, X.; Yao, L. Q.; Zhang, Y.; Fan, Z. W.; Cheng, Y.; Liu, X.; Wu, F. Q.; Qin, S.; Yan, Y. Y.; Ding, F.; Liu, W.; Zhu, K. G.; Liu, D. T.; Qi, S. H. Temperature dependence of source profiles for volatile organic compounds from typical volatile emission sources. *Sci. Total Environ.* **2021**, *751*, No. 141741.

(11) Qi, Y. Q.; Shen, L. M.; Zhang, J. L.; Yao, J.; Lu, R.; Miyakoshi, T. Species and release characteristics of VOCs in furniture coating process. *Environ. Pollut.* **2019**, *245*, 810−819.

(12) Rubin, J. I.; Kean, A. J.; Harley, R. A.; Millet, D. B.; Goldstein, A. H. Temperature dependence of volatile organic compound evaporative emissions from motor vehicles. *Journal of Geophysical Research-Atmospheres* **2006**, *111* (D3), No. D03305.

(13) Zheng, H.; Kong, S.; Xing, X.; Mao, Y.; Hu, T.; Ding, Y.; Li, G.; Liu, D.; Li, S.; Qi, S. Monitoring of volatile organic compounds (VOCs) from an oil and gas station in northwest China for 1 year. *Atmospheric Chemistry and Physics* **2018**, *18* (7), 4567−4595.

(14) Song, C. B.; Liu, B. S.; Dai, Q. L.; Li, H. R.; Mao, H. J. Temperature dependence and source apportionment of volatile organic compounds (VOCs) at an urban site on the north China plain. *Atmos. Environ.* **2019**, *207*, 167−181.

(15) Na, K.; Moon, K. C.; Kim, Y. P. Source contribution to aromatic VOC concentration and ozone formation potential in the atmosphere of Seoul. *Atmos. Environ.* **2005**, *39* (30), 5517−5524.

(16) Gu, Y. X.; Li, K.; Xu, J. M.; Liao, H.; Zhou, G. Q. Observed dependence of surface ozone on increasing temperature in Shanghai, China. *Atmos. Environ.* **2020**, *221*, No. 117108.

(17) Feng, X.; Lin, H. P.; Fu, T. M.; Sulprizio, M. P.; Zhuang, J. W.; Jacob, D. J.; Tian, H.; Ma, Y. P.; Zhang, L. J.; Wang, X. L.; Chen, Q.; Han, Z. W. WRF-GC (v2.0): online two-way coupling of WRF (v3.9.1.1) and GEOS-Chem (v12.7.2) for modeling regional atmospheric chemistry-meteorology interactions. *Geoscientific Model Development* **2021**, *14* (6), 3741−3768.

(18) Lin, H. P.; Feng, X.; Fu, T. M.; Tian, H.; Ma, Y. P.; Zhang, L. J.; Jacob, D. J.; Yantosca, R. M.; Sulprizio, M. P.; Lundgren, E. W.; Zhuang, J. W.; Zhang, Q.; Lu, X.; Zhang, L.; Shen, L.; Guo, J. P.; Eastham, S. D.; Keller, C. A. WRF-GC (v1.0): online coupling of WRF (v3.9.1.1) and GEOS-Chem (v12.2.1) for regional atmospheric chemistry modeling - Part 1: Description of the one-way model. *Geoscientific Model Development* **2020**, *13* (7), 3241−3265.

(19) Skamarock, W. C.; Klemp, J. B. A time-split nonhydrostatic atmospheric model for weather research and forecasting applications. *J. Comput. Phys.* **2008**, *227* (7), 3465−3485.

(20) Bey, I.; Jacob, D. J.; Yantosca, R. M.; Logan, J. A.; Field, B. D.; Fiore, A. M.; Li, Q. B.; Liu, H. G. Y.; Mickley, L. J.; Schultz, M. G. Global modeling of tropospheric chemistry with assimilated meteorology: Model description and evaluation. *Journal of Geophysical Research-Atmospheres* **2001**, *106* (D19), 23073−23095.

(21) Bates, K. H.; Jacob, D. J.; Li, K.; Ivatt, P. D.; Evans, M. J.; Yan, Y. Y.; Lin, J. T. Development and evaluation of a new compact mechanism for aromatic oxidation in atmospheric models. *Atmospheric Chemistry and Physics* **2021**, *21* (24), 18351−18374.

(22) NCEP FNL operational model global tropospheric analyses, continuing from July 1999. *Research Data Archive at the National Center for Atmospheric Research, Computational and Information Systems Laboratory*. https://doi.org/10.5065/D6M043C6 (accessed January 2023).

(23) Li, M.; Zhang, Q.; Streets, D. G.; He, K. B.; Cheng, Y. F.; Emmons, L. K.; Huo, H.; Kang, S. C.; Lu, Z.; Shao, M.; Su, H.; Yu, X.; Zhang, Y. Mapping Asian anthropogenic emissions of non-methane volatile organic compounds to multiple chemical mechanisms. *Atmospheric Chemistry and Physics* **2014**, *14* (11), 5617−5638.

(24) Zheng, B.; Tong, D.; Li, M.; Liu, F.; Hong, C. P.; Geng, G. N.; Li, H. Y.; Li, X.; Peng, L. Q.; Qi, J.; Yan, L.; Zhang, Y. X.; Zhao, H. Y.; Zheng, Y. X.; He, K. B.; Zhang, Q. Trends in China's anthropogenic emissions since 2010 as the consequence of clean air actions. *Atmospheric Chemistry and Physics* **2018**, *18* (19), 14095−14111.

(25) Li, M.; Zhang, Q.; Kurokawa, J.; Woo, J. H.; He, K. B.; Lu, Z. F.; Ohara, T.; Song, Y.; Streets, D. G.; Carmichael, G. R.; Cheng, Y. F.; Hong, C. P.; Huo, H.; Jiang, X. J.; Kang, S. C.; Liu, F.; Su, H.; Zheng, B. MIX: A mosaic Asian anthropogenic emission inventory under the international collaboration framework of the MICS-Asia and HTAP. *Atmospheric Chemistry and Physics* **2017**, *17* (2), 935−963.

(26) Van der werf, G. R.; Randerson, J. T.; Giglio, L.; Van leeuwen, T. T.; Chen, Y.; Rogers, B. M.; Mu, M.; Van marle, M. J. E.; Morton, D. C.; Collatz, G. J.; Yokelson, R. J.; Kasibhatla, P. S. Global fire emissions estimates during 1997−2016. *Earth System Science Data* **2017**, *9* (2), 697−720.

(27) Hudman, R. C.; Moore, N. E.; Mebust, A. K.; Martin, R. V.; Russell, A. R.; Valin, L. C.; Cohen, R. C. Steps towards a mechanistic model of global soil nitric oxide emissions: Implementation and space based-constraints. *Atmospheric Chemistry and Physics* **2012**, *12* (16), 7779−7795.

(28) Murray, L. T.; Jacob, D. J.; Logan, J. A.; Hudman, R. C.; Koshak, W. J. Optimized regional and interannual variability of lightning in a global chemical transport model constrained by LIS/OTD satellite data. *Journal of Geophysical Research-Atmospheres* **2012**, *117* (D20), No. D20307.

(29) Atkins, P. W. *Physical Chemistry*; Oxford University Press, 1998.

(30) Romagnuolo, L.; Yang, R. C.; Frosina, E.; Rizzoni, G.; Andreozzi, A.; Senatore, A. Physical modeling of evaporative emission control system in gasoline fueled automobiles: A review. *Renewable & Sustainable Energy Reviews* **2019**, *116*, No. 109462.

(31) Liu, H.; Man, H. Y.; Cui, H. Y.; Wang, Y. J.; Deng, F. Y.; Wang, Y.; Yang, X. F.; Xiao, Q.; Zhang, Q.; Ding, Y.; He, K. B. An updated

https://doi.org/10.1021/acs.est.3c09122
Environ. Sci. Technol. 2024, 58, 5430−5441

emission inventory of vehicular VOCs and IVOCs in China. *Atmospheric Chemistry and Physics* **2017**, *17* (20), 12709−12724.
(32) Huang, J.; Yuan, Z.; Duan, Y.; Liu, D.; Fu, Q.; Liang, G.; Li, F.; Huang, X. Quantification of temperature dependence of vehicle evaporative volatile organic compound emissions from different fuel types in China. *Sci. Total Environ.* **2022**, *813*, No. 152661.
(33) Huang, S. D.; Xiong, J. Y.; Zhang, Y. P. Impact of temperature on the ratio of initial emittable concentration to total concentration for formaldehyde in building materials: theoretical correlation and validation. *Environ. Sci. Technol.* **2015**, *49* (3), 1537−1544.
(34) Yamada, H.; Inomata, S.; Tanimoto, H. Refueling emissions from cars in Japan: Compositions, temperature dependence and effect of vapor liquefied collection system. *Atmos. Environ.* **2015**, *120*, 455−462.
(35) Yamada, H.; Inomata, S.; Tanimoto, H.; Hata, H.; Tonokura, K. Estimation of refueling emissions based on theoretical model and effects of E10 fuel on refueling and evaporative emissions from gasoline cars. *Sci. Total Environ.* **2018**, *622*, 467−473.
(36) Ministry of Ecology and Environment of the People's Republic of China (MEE). *China Mobile Source Environmental Management Annual Report*; 2019. https://www.mee.gov.cn/hjzl/sthjzk/ydyhjgl/201909/P020190905586230826402.pdf (accessed February 2023).
(37) Tan, Y. Y.; Zhi, Y. T.; Gao, M. P.; Cheng, Z. J.; Yan, B. B.; Nie, L.; Chen, G. Y.; Hou, L. A. Influence of temperature on formaldehyde emission parameters of solvent-based coatings. *Journal of Coatings Technology and Research* **2021**, *18* (3), 677−684.
(38) Xiong, J.; Wei, W.; Huang, S.; Zhang, Y. Association between the emission rate and temperature for chemical pollutants in building materials: general correlation and understanding. *Environ. Sci. Technol. Lett.* **2013**, *47* (15), 8540−8547.
(39) Liang, Z.; Yu, Y.; Sun, B.; Yao, Q.; Lin, X.; Wang, Y.; Zhang, J.; Li, Y.; Wang, X.; Tang, Z.; Ma, S. The underappreciated role of fugitive VOCs in ozone formation and health risk assessment emitted from seven typical industries in China. *Journal of Environmental Sciences* **2024**, *136*, 647−657.
(40) Carter, W. P. L. Development of ozone reactivity scales for volatile organic-compounds. *J. Air Waste Manage. Assoc.* **1994**, *44* (7), 881−899.
(41) Wu, R. R.; Xie, S. D. Spatial distribution of ozone formation in China derived from emissions of speciated volatile organic compounds. *Environ. Sci. Technol.* **2017**, *51* (5), 2574−2583.
(42) Zheng, J.; Shao, M.; Che, W.; Zhang, L.; Zhong, L.; Zhang, Y.; Streets, D. Speciated VOC emission inventory and spatial patterns of ozone formation potential in the Pearl River Delta, China. *Environ. Sci. Technol.* **2009**, *43* (22), 8580−8586.
(43) Carter, W. P. L. Development of the SAPRC-07 chemical mechanism. *Atmos. Environ.* **2010**, *44* (40), 5324−5335.
(44) Zhang, Y. N.; Xue, L. K.; Carter, W. P. L.; Pei, C. L.; Chen, T. S.; Mu, J. S.; Wang, Y. J.; Zhang, Q. Z.; Wang, W. X. Development of ozone reactivity scales for volatile organic compounds in a Chinese megacity. *Atmospheric Chemistry and Physics* **2021**, *21* (14), 11053−11068.
(45) Zhang, Y. N.; Xue, L. K.; Mu, J. S.; Chen, T. S.; Li, H.; Gao, J.; Wang, W. X. Developing the maximum incremental reactivity for Volatile Organic Compounds in major cities of central-eastern China. *Journal of Geophysical Research-Atmospheres* **2022**, *127* (22), No. e2022JD037296.
(46) Duncan, B. N.; Yoshida, Y.; Olson, J. R.; Sillman, S.; Martin, R. V.; Lamsal, L.; Hu, Y. T.; Pickering, K. E.; Retscher, C.; Allen, D. J.; Crawford, J. H. Application of OMI observations to a space-based indicator of NOx and VOC controls on surface ozone formation. *Atmos. Environ.* **2010**, *44* (18), 2213−2223.
(47) Jin, X. M.; Fiore, A. M.; Murray, L. T.; Valin, L. C.; Lamsal, L. N.; Duncan, B.; Folkert boersma, K.; De smedt, I.; Abad, G. G.; Chance, K.; Tonnesen, G. S. Evaluating a space-based indicator of surface ozone-NO_x-VOC sensitivity over midlatitude source regions and application to decadal trends. *Journal of Geophysical Research-Atmospheres* **2017**, *122* (19), 10231−10253.
(48) Martin, R. V.; Fiore, A. M.; Van donkelaar, A. Space-based diagnosis of surface ozone sensitivity to anthropogenic emissions. *Geophys. Res. Lett.* **2004**, *31* (6), No. L06120.
(49) OMI/Aura NO2 L3 Global Gridded 0.25 degree x 0.25 degree V3. *National Aeronautics and Space Administration (NASA), Goddard Space Flight Center, Goddard Earth Sciences Data and Information Services Center (GES DISC)*. 10.5067/Aura/OMI/DATA3007 (accessed January 2023).
(50) *OMI/Aura Formaldehyde (HCHO) Total Column Daily L3 Weighted Mean Global 0.1deg Lat/Lon Grid V003. National Aeronautics and Space Administration (NASA), Goddard Earth Sciences Data and Information Services Center (GES DISC)*. 10.5067/Aura/OMI/DATA3010 (accessed January 2023).
(51) Wang, T.; Xue, L. K.; Brimblecombe, P.; Lam, Y. F.; Li, L.; Zhang, L. Ozone pollution in China: A review of concentrations, meteorological influences, chemical precursors, and effects. *Sci. Total Environ.* **2017**, *575*, 1582−1596.
(52) Li, K.; Jacob, D. J.; Shen, L.; Lu, X.; De smedt, I.; Liao, H. Increases in surface ozone pollution in China from 2013 to 2019: Anthropogenic and meteorological influences. *Atmospheric Chemistry and Physics* **2020**, *20* (19), 11423−11433.
(53) Bates, K. H.; Jacob, D. J. A new model mechanism for atmospheric oxidation of isoprene: Global effects on oxidants, nitrogen oxides, organic products, and secondary organic aerosol. *Atmospheric Chemistry and Physics* **2019**, *19* (14), 9613−9640.
(54) Sakamoto, Y.; Kohno, N.; Ramasamy, S.; Sato, K.; Morino, Y.; Kajii, Y. Investigation of OH-reactivity budget in the isoprene, a-pinene and m-xylene oxidation with OH under high NO_x conditions. *Atmos. Environ.* **2022**, *271*, No. 118916.
(55) Ye, L.; Wang, X.; Fan, S.; Chen, W.; Chang, M.; Zhou, S.; Wu, Z.; Fan, Q. Photochemical indicators of ozone sensitivity: application in the Pearl River Delta, China. *Frontiers of. Environmental Science & Engineering* **2016**, *10* (6), No. 15.
(56) Wang, W.; Ronald, V. D. A.; Ding, J.; van Weele, M.; Cheng, T. Spatial and temporal changes of the ozone sensitivity in China based on satellite and ground-based observations. *Atmos. Chem. Phys.* **2021**, *21* (9), 7253−7269.
(57) Fu, T. M.; Zheng, Y. Q.; Paulot, F.; Mao, J. Q.; Yantosca, R. M. Positive but variable sensitivity of August surface ozone to large-scale warming in the southeast United States. *Nature Climate Change* **2015**, *5* (5), 454−458.
(58) Porter, W. C.; Heald, C. L. The mechanisms and meteorological drivers of the summertime ozone-temperature relationship. *Atmospheric Chemistry and Physics* **2019**, *19* (20), 13367−13381.
(59) Lu, Q.; Zhao, Y.; Robinson, A. L. Comprehensive organic emission profiles for gasoline, diesel, and gas-turbine engines including intermediate and semi-volatile organic compound emissions. *Atmospheric Chemistry and Physics* **2018**, *18* (23), 17637−17654.
(60) Ministry of Ecology and Environment of the People's Republic of China (MEE). *"Fourteenth Five-Year Plan" for Ecological Environment Monitoring*; 2021. https://www.mee.gov.cn/xxgk2018/xxgk/xxgk03/202201/W020220121627956920736.pdf (accessed January 2024).
(61) Ministry of Ecology and Environment of the People's Republic of China (MEE). *Limits and measurement method for emissions from light-duty vehicles (CHINA 6)*; 2016. https://www.mee.gov.cn/ywgz/fgbz/bz/bzwb/dqhjbh/dqydywrwpfbz/201612/W020171207355626647621.pdf (accessed January 2024).
(62) China State Council. *NEV Industry Development Plan (2021−2035)*; 2020. https://www.gov.cn/zhengce/content/2020-11/02/content_5556716.htm (accessed January 2024).
(63) Petersen, A. K.; Brasseur, G. P.; Bouarar, I.; Flemming, J.; Gauss, M.; Jiang, F.; Kouznetsov, R.; Kranenburg, R.; Mijling, B.; Peuch, V. H.; Pommier, M.; Segers, A.; Sofiev, M.; Timmermans, R.; Van der, A. R.; Walters, S.; Xie, Y.; Xu, J. M.; Zhou, G. Q. Ensemble forecasts of air quality in eastern China - Part 2: Evaluation of the

https://doi.org/10.1021/acs.est.3c09122
Environ. Sci. Technol. 2024, 58, 5430−5441

MarcoPolo-Panda prediction system, version 1. *Geosci. Model Dev.* **2019**, *12* (3), 1241−1266.
(64) Yang, J. Y.; Zhao, Y. Performance and application of air quality models on ozone simulation in China - A review. *Atmos. Environ.* **2023**, *293*, No. 119446.
(65) Ministry of Ecology and Environment of People's Republic of China (MEE). *Notice on Issuing "the Action Plan for Deepening the Fight against Heavy Polluted Weather Elimination, Ozone Pollution Prevention and Control, and Diesel Truck Pollution Control*; 2022. https://www.mee.gov.cn/xxgk2018/xxgk/xxgk03/202211/t20221161005042.html (accessed May 2023).
(66) Perkins-kirkpatrick, S. E.; Lewis, S. C. Increasing trends in regional heatwaves. *Nature. Communications* **2020**, *11* (1), No. 3357.
(67) Wang, Y.; Ge, C.; Castro garcia, L.; Jenerette, G. D.; Oikawa, P. Y.; Wang, J. Improved modelling of soil NO_x emissions in a high temperature agricultural region: role of background emissions on NO_x trend over the US. *Environmental Research Letters* **2021**, *16* (8), No. 084061.
(68) Gunawardena, K. R.; Wells, M. J.; Kershaw, T. Utilising green and bluespace to mitigate urban heat island intensity. *Sci. Total Environ.* **2017**, *584*, 1040−1055.
(69) Schlaerth, H. L.; Silva, S. J.; Li, Y. Characterizing ozone sensitivity to urban greening in Los Angeles under current day and future anthropogenic emissions scenarios. *Journal of Geophysical Research-Atmospheres* **2023**, *128* (20), No. e2023JD039199.
(70) Yu, M.; Zhou, W.; Zhao, X.; Liang, X.; Wang, Y.; Tang, G. Is urban greening an effective solution to enhance environmental comfort and improve air quality? *Environmental Science & Technology Letters* **2022**, *56* (9), 5390−5397.

https://doi.org/10.1021/acs.est.3c09122
Environ. Sci. Technol. 2024, 58, 5430−5441